Computational Studies of the Geometry and Electronic Structure of an All-Inorganic and Homogeneous Tetra-Ru-Polyoxotungstate Catalyst for Water Oxidation and Its Four Subsequent On...

ARTICLE *in* THE JOURNAL OF PHYSICAL CHEMISTRY A · DECEMBER 2009

Impact Factor: 2.69 · DOI: 10.1021/jp907471h · Source: PubMed

Computational Studies of the Geometry and Electronic Structure of an All-Inorganic and Homogeneous Tetra-Ru-Polyoxotungstate Catalyst for Water Oxidation and Its Four Subsequent One-Electron Oxidized Forms

David Quiñonero,[†] Alexey L. Kaledin, Aleksey E. Kuznetsov, Yurii V. Geletii, Claire Besson,[‡] Craig L. Hill, and Djamaladdin G. Musaev*

Cherry L. Emerson Center for Scientific Computation, and Department of Chemistry, Emory University, Atlanta, Georgia 30322

Received: August 3, 2009; Revised Manuscript Received: October 5, 2009

Geometry and electronic structure of five species $[\{Ru_4O_4(OH)_2(H_2O)_4\}(\gamma\text{-}SiW_{10}O_{36})_2]^{10-}$ (**1**), $[\{Ru_4O_4(OH)_2(H_2O)_4\}(\gamma\text{-}SiW_{10}O_{36})_2]^{9-}$ (**2**), $[\{Ru_4O_4(OH)_2(H_2O)_4\}(\gamma\text{-}SiW_{10}O_{36})_2]^{8-}$ (**3**), $[\{Ru_4O_4(OH)_2(H_2O)_4\}(\gamma\text{-}SiW_{10}O_{36})_2]^{7-}$ (**4**), and $[\{Ru_4O_4(OH)_2(H_2O)_4\}(\gamma\text{-}SiW_{10}O_{36})_2]^{6-}$ (**5**) with different oxidation states of Ru centers were studied at the density functional and COSMO levels of theory. These species are expected to be among the possible intermediates of the recently reported **1**-catalyzed water oxidation (Geletii, Y. V.; Botar, B.; Kögerler, P.; Hillesheim, D. A.; Musaev, D. G.; Hill, C. L. *Angew. Chem. Int. Ed.* **2008**, *47*, 3896−3899 and Sartorel, A.; Carraro, M.; Scorrano, G.; Zorzi, R. D.; Geremia, S.; McDaniel, N. D.; Bernhard, S.; Bonchio, M. *J. Am. Chem. Soc*. **2008**, *130*, 5006−5007). It was shown that RI-BP86 correctly describes the geometry and energy of the low-lying electronic states of compound **1**, whereas the widely used B3LYP approach overestimates the energy of its high-spin states. Including the solvent and/or countercation effects into calculations improves the agreement between the calculated and experimental data. It was found that the several HOMOs and LUMOs of the studied complexes are bonding and antibonding orbitals of the $[Ru_4O_4(OH)_2(H_2O)_4]^{6+}$ core, and four subsequent one-electron oxidations of **1,** leading to formation of **2, 3, 4**, and **5**, respectively, involve only $\{Ru_4\}$ core orbitals. In other words, catalyst instability due to ligand oxidation in the widely studied Ru-blue dimer, $[(bpy)_2(O)Ru^{V}\text{-}(\mu\text{-}O)\text{-}Ru^{V}(O)(bpy)_2]^{4+}$, is not operable for **1**: the latter all-inorganic catalyst is predicted to be stable under water oxidation turnover conditions. The calculated HOMOs and LUMOs of all the studied species are very close in energy and exhibit a "quasi-continuum" or "nanoparticle-type" electronic structure similar to that of nanosized transition metal clusters. This conclusion closely correlates with the experimentally reported oxidation and reduction features of **1** and explains the unusual linear dependence of oxidation potential versus charges for these compounds. The decrease in total negative charge of the system via **1** > **2** > **3** > **4** > **5**, on average, decreases the $\{Ru_4\}-\{SiW_{10}\}$ distance. It is predicted that at higher pH compound **1** will, initially, release protons from the $\mu\text{-}O_{Ru}$ oxygen centers.

Introduction

The development of efficient molecular catalysts for oxidation of water is of great importance and has been the recent focus of numerous highly active research groups. Many multinuclear transition metal complexes with varying degrees of catalytic water oxidation activity have been reported.[1−24] However, the presence of organic ligands in nearly all these compounds render them oxidatively unstable under turnover conditions. Recently, our group reported[23] the Rb_8K_2 salt of a new complex, $[\{Ru_4O_4(OH)_2(H_2O)_4\}(\gamma\text{-}SiW_{10}O_{36})_2]^{10-}$ (**1**), free of organic components, that exhibits several reversible one-electron redox couples by cyclic voltammetry over a narrow potential range and catalyzes both the electro-oxidation and chemical oxidation of water in aqueous solution at low overpotentials. Simultaneously, Bonchio and co-workers developed the same catalyst.[24] The two reports differ by the oxidant and pH of operation and the salt used to obtain the X-ray structure: our study used $[Ru(bpy)_3]^{3+}$ as the oxidant at pH 7 and their study used Ce^{4+} as the oxidant at pH 1.8.

Our previous studies[23] indicated that in the resting state (in the absence of an external oxidant) the oxidation state of all four ruthenium centers in **1** are 4+. However, the oxidation states of these metal centers in intermediates involved in water oxidation, as well as the mechanism of O_2 formation itself in this system, still remain unclear. Previously, based on reaction thermodynamics and kinetics, we proposed the intermediacy of species containing one Ru^{V} and three Ru^{IV}, two Ru^{V} and two Ru^{IV}, three Ru^{V} and one Ru^{IV}, and four Ru^{V} centers, referred to hereafter in this paper as **2**, **3**, **4**, and **5**, respectively. Unfortunately, the nature of these species is unknown.

We report here computational studies on the geometry and electronic structure of $[\{Ru_4O_4(OH)_2(H_2O)_4\}(\gamma\text{-}SiW_{10}O_{36})_2]^{10-}$ (**1**), $[\{Ru_4O_4(OH)_2(H_2O)_4\}(\gamma\text{-}SiW_{10}O_{36})_2]^{9-}$ (**2**), $[\{Ru_4O_4(OH)_2(H_2O)_4\}(\gamma\text{-}SiW_{10}O_{36})_2]^{8-}$ (**3**), $[\{Ru_4O_4(OH)_2(H_2O)_4\}(\gamma\text{-}SiW_{10}O_{36})_2]^{7-}$ (**4**), and $[\{Ru_4O_4(OH)_2(H_2O)_4\}(\gamma\text{-}SiW_{10}O_{36})_2]^{6-}$ (**5**).

Computational Methods

Initially, geometry optimization of all compounds under study was performed without any symmetry constraints. However, upon the geometry optimization even-charged species converged

* To whom correspondence should be addressed. E-mail- dmusaev@emory.edu. Phone: 1-404-727-2382.

[†] Current address: Departament de Química, Universitat de les Illes Balears, Crta. de Valldemossa km 7.5, 07122 Palma de Mallorca, Spain.

[‡] Current address: Institut Parisien de Chimie Moléculaire, UPMC University Paris 06 Case 42, 4 Place Jussieu 75252 Paris Cedex 5, France.

10.1021/jp907471h
Published on Web 12/03/2009

TABLE 1: Energy Differences (ΔE, in kcal/mol) between the Lower-Lying Electronic States of the Compounds 1−5 Calculated at the RI-BP86/DZ Level of Theory (Unless Otherwise Stated) Using the D_2 Symmetry

structure	states	ΔE	structure	states	ΔE	structure	states	ΔE
1	singlet	0.0	2	doublet	0.0	**3**	triplet	0.0
	quintet	19.6		quartet	6.1		septet	17.8
	nonatet	15.8		decitet	21.3		undecitet	22.5
		15.8[a]						
		15.8[b]						
		17.7[c]						
		−21.3[d]						
4	quartet	0.0	5	quintet	0.0			
	sextet	4.1		nonatet	8.1			
					8.1[a]			
	duodecitet	17.6		tredecitet	28.7			
					35.2[a]			

[a] At the D_{2d} symmetry. [b] At the C_2 symmetry. [c] At the C_2 symmetry using the TZ basis sets. [d] RI-B3LYP/DZ//RI-BP86/DZ results using D_{2d} symmetry.

to C_2 symmetry structures. Therefore C_2 symmetry was used for these species, unless stated otherwise. In these calculations we used the BP86 density functional[25,26] in conjunction with the Ahlrichs triple-ζ basis sets for all atoms and the associated effective core potentials for Ru and W (def-TZVP basis set, TZ hereafter),[27] unless stated otherwise. The reported BP86 calculations were carried out at the resolution of the identity (RI) level. We have used the parallel RI-DFT[28,29] methodology, which uses an auxiliary fitting basis to avoid treating the complete set of two-electron repulsion integrals, thus speeding up calculations significantly.

The environment effects (with water as solvent) were taken into account at the Conductor-like Screening Model (COSMO)[30] level of theory. For all compounds we have carried out geometry optimization in water at the RI-BP86/TZ level.

All reported calculations (unless stated otherwise, see section on the studies of countercation effects) were performed using the TURBOMOLE software, version 5.10.[31] Molecular orbitals of the optimized structures were visualized using Molden 4.1.[32]

We explored the low-lying spin states of each reported compound using high symmetry (D_{2d}, D_2) except for compounds **2** and **4**, where no symmetry constraints were applied. In these calculations, we used the Ahlrichs double-ζ basis set for all atoms with the associated effective core potentials for Ru and W (def-SVP basis set, DZ hereafter).[33] The results are summarized in Table 1.

As seen from the table, the low-spin states for all the studied compounds are found to be the ground states, i.e., singlet, doublet, triplet, quartet, and quintet states for **1**, **2**, **3**, **4**, and **5**, respectively. To validate these conclusions obtained at the RI-BP86/DZ level, we studied the electronic states of compound **1** by employing relatively large TZ basis set without imposing any symmetry constraints. It was found that regardless of the basis set (DZ or TZ) and the symmetry used, the energy ordering of spin states was the same. Therefore, below we extensively investigate the energy gap between numerous low-lying electronic states of the studied compounds at the less expensive RI-BP86/DZ level of theory. After establishing the ground electronic states of these species, their geometries and physical and chemical properties were investigated at the RI-BP86/TZ and COSMO-RI-BP86/TZ levels of theory. Full Cartesian coordinates of all calculated structures are given in Table S1 of the Supporting Information.

We also tested the applicability of the widely used hybrid B3LYP functional[34] for the compounds under study by performing RI-B3LYP/DZ single-point calculations on the RI-BP86/DZ optimized singlet and nonatet states of **1** in D_{2d} symmetry. As seen in Table 1, the RI-B3LYP/DZ approach predicts the nonatet ground state, which is 21.3 kcal/mol lower in energy than the singlet state. This finding is not consistent with the results obtained at the RI-BP86 level and in experiments.[23] Indeed, experiments establish that compound **1** is diamagnetic with four Ru^{IV} centers.[23,24] Thus, the agreement between calculated and experimental data for the complex **1** clearly favors the nonhybrid RI-BP86 method. Therefore, below we discuss only the results obtained at this level of theory.

One should note that the compounds investigated, structures **1**−**5**, all have a large negative charge, and the better description of their oxidation and reduction potentials requires basis sets larger than TZ with diffuse functions. Unfortunately, the TZ basis sets used in this paper are relatively small and do not include diffuse functions, and may lead to incorrect oxidation and reduction energies of these compounds. For this reason, below, we will not discuss these values, but will mainly focus on the calculated geometries, frontier orbitals, and NPA analysis of these species, which could be properly described at the RI-B3LYP/TZ level of theory.

Results and Discussion

Compound 1, $[\{Ru_4O_4(OH)_2(H_2O)_4\}(\gamma\text{-}SiW_{10}O_{36})_2]^{10-}$. The total charge of compound **1** is defined to be 10−, which is consistent with all four Ru centers in oxidation state 4+. Our calculations at the RI-BP86/DZ level of theory show that the ground state of this compound is a singlet, which is in good agreement with the available experimental data.[23] We have recalculated the ground singlet electronic state of this compound using both restricted and unrestricted RI-BP86/TZ formalisms, and in both cases the same results were obtained. Below, we discuss only the restricted-RI-BP86/TZ calculated results. We start our discussion with analysis of the geometric structure of **1**. Labeling of selected atoms is depicted in Figure 1. As seen from the figure, compound **1** can be considered as a $[Ru_4O_4(OH)_2(H_2O)_4]^{6+}$ core (below referred to as $\{Ru_4\}$) sandwiched between two staggered $\{SiW_{10}\}^{8-}$ monomeric units, where the four Ru centers of the $\{Ru_4\}$ core form a slightly distorted tetrahedron.

For simplicity of the discussion we divide the oxygen atoms of the $\{Ru_4\}$ core into four groups: (i) μ-O_{Ru} in Ru−O−Ru, (ii) μ−OH_{Ru} in Ru−OH−Ru, (iii) μ-O_W in Ru−O−W, and (iv) O_{water} in Ru−OH_2 fragments. In the Ru−O−Ru fragments two sets of Ru−O_{Ru} bond distances can be identified: (i) bond

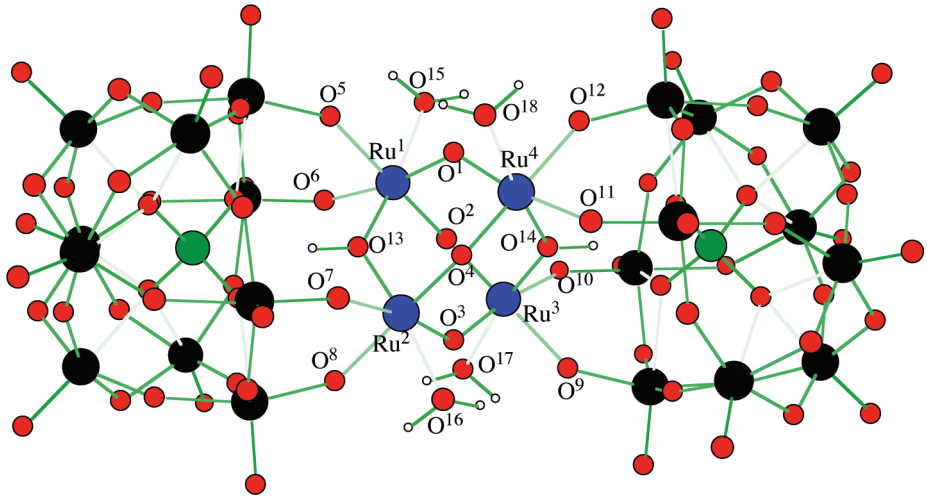

Figure 1. Calculated structure of complex **1** and the labeling scheme for atoms of the $\{Ru_4O_4(OH)_2(H_2O)_4\}$ core.

distances involving the O^3 and O^1 atoms with no H-bonding, and (ii) bond distances involving O^2 and O^4 atoms H-bonded (by one of H-atom each, O−H bond distances 2.186 Å) to two water molecules coordinated to Ru^1 and Ru^2 centers (see Table 2). As expected, the first set of $Ru-O_{Ru}$ bond distances, 1.853−1.854 Å, are slightly shorter than the second set, 1.926 Å. The $Ru-OH_{Ru}$ distances are very similar with values of 1.971−1.974 Å, which are ca. 0.12 Å longer than $Ru-O_{Ru}$ bond distances. The calculated $Ru-O_W$ bond distances are almost identical (2.082−2.083 Å). As anticipated, the longest Ru−O bond distances in the $\{Ru_4\}$ core correspond to the $Ru-OH_2$ bonds (2.257−2.260 Å).

Inclusion of the solvent effects into calculations at the COSMO level changes geometry parameters obtained in gas-phase: the observed difference among the Ru−Ru distances increases, now, they range from 3.504 Å (3.544 Å in the gas-phase) to 3.636 Å (3.570 Å in the gas-phase), resulting in a more distorted tetrahedral geometry for the $\{Ru_4\}$ core. The calculated $Ru-O_{Ru}$ bond distances involving the O^3 and O^1 atoms, are very similar in the gas-phase and in water. However, the $Ru-O_{Ru}$ bond distances, involving H-bonded O^2 and O^4 atoms, are slightly shorter in solution due to the solvent screening effect that weakens the hydrogen bonding (this O−H bond distance is 2.596 Å). The $Ru-OH_{Ru}$ bond distances are elongated by 0.02 Å to 1.993−1.994 Å in solution. The $Ru-O_W$ bond distances (2.053−2.068 Å) are slightly shorter than in the gas-phase. Finally, the $Ru-OH_2$ bond distances are shorter by ca. 0.06 Å compared to the gas-phase. In general, the geometry parameters retrieved from the COSMO calculations are closer to the reported X-ray structure.[23] This can be rationalized from the electrostatic point of view: in the crystal structure, polyanion **1** is surrounded by countercations (8 Rb^+ and 2 K^+), whereas in the continuum solvation model employed it is surrounded by a dielectric continuum composed of water molecules. Thus, inclusion of electrostatic interactions between **1** and its surroundings improves the agreement between the experimental and calculated values of geometry parameters of **1**.

We have calculated NPA charges for selected atoms of **1**; these are presented in Table 3.

In the gas-phase, the calculated NPA charges of Ru atoms are 1.18−1.19e. The negative charge of the polyanion unit is exclusively distributed among its oxygen atoms. From the selected oxygen atoms of the $\{Ru_4\}$ core, those belonging to the coordinated water molecules, $O^{15}-O^{18}$, have the highest negative charge (−0.84e). Within the Ru−O−Ru groups, the charge of the O centers involved in hydrogen bonding with the water molecules, O^2 and O^4, is more negative (−0.65e) than the charge of the O centers without H-bonding, O^1 and O^3 (−0.40e and −0.39e). The oxygen atoms of the Ru−OH−Ru groups are slightly more negatively charged (−0.68e) compared to oxygens of the Ru−O−Ru groups. Meanwhile, the O atoms of the Ru−O−W groups bear larger negative charges than the O atoms of the Ru−OH−Ru group. In fact, the O atoms of Ru−OH−Ru groups could be divided into two sets according to their charges: the oxygens with the hydrogen-bonding pattern (O−H bond distance 1.885 Å) bear a charge of −0.80e, whereas the other oxygens of this group have a smaller charge, −0.68e. Thus, basicity of the oxygen centers of the $\{Ru_4\}$ core and oxygens located in the vicinity of this core increases as μ-O_{Ru} < $\mu-OH_{Ru}$ < μ-O_W < O_{water}. Based on this finding one may predict that at higher pH the system will likely first release protons from the μ-OH_{Ru} oxygen centers, and could exist at its $[\{Ru_4O_6(H_2O)_4\}(\gamma\text{-}SiW_{10}O_{36})_2]^{12-}$ form.

As seen in Table 3, inclusion of the solvent effects did not change the charges on the Ru centers (1.18e) and on the O atoms of OH moieties (−0.70e) (i.e., in Ru−OH−Ru groups) and water molecules (−0.82e). However, in aqueous solution, charges on the μ-O_{Ru} atoms *with* H-bonds are decreased from −0.65e to −0.52e. On the contrary, charges on the μ-O_{Ru} atoms *without* H-bonds are increased from −0.40e to −0.44e. These data suggest that the charges of the μ-O_{Ru} atoms tend to be equalized due to the solvent effects. This is also true for the charges of the μ-O_W atoms: in solution, the charge on the μ-O_W atoms with and without hydrogen bonding decreases to −0.73e and increases to −0.70e, respectively.

In Figure 2 we show the highest occupied (HOMO − 4 to HOMO) and the lowest unoccupied molecular orbitals (LUMO to LUMO + 4) of compound **1** in the gas-phase. Their corresponding energies are given in Table 4.

As seen from Figure 2, all four HOMOs have significant contributions from only the atoms of the $[Ru_4(\mu\text{-}O)_4(\mu\text{-}OH)_2(H_2O)_4]^{6+}$ core. This phenomenon is also operable for the LUMOs with the exception of LUMO + 4. The main contributions to this orbital derive from the {W−O} framework orbitals. The calculated MO energies are quite informative also. The energy gap between HOMO and HOMO − 4 is only 0.34 eV. The same picture retains for the LUMOs, the bottom five being clustered within 1.17 eV (and the bottom four between 0.435 eV). The calculated HOMO−LUMO gap is only 0.316 eV. Inclusion of the solvent and countercation effects, which

TABLE 2: Important Bond Distances (in Å) in the $Ru_4(\mu\text{-}O)_4(\mu\text{-}OH)_2(H_2O)_4$ Core of the Complexes 1-5, Calculated in the Gas-Phase and in Water Solution (in italic), and Comparison of the Calculated Geometry Parameters with Their Experimental Values [ref 23] for Complex 1[a]

bond	5	4	3	2	1	X-ray
Ru^1-Ru^2	3.639	3.592	3.577	3.554	3.570	3.660
	3.659	*3.650*	*3.628*	*3.630*	*3.636*	
Ru^1-Ru^3	3.627	3.600	3.544	3.547	3.566	3.470
	3.555	*3.593*	*3.484*	*3.489*	*3.504*	
Ru^1-Ru^4	3.570	3.554	3.607	3.606	3.547	3.541
	3.584	*3.545*	*3.581*	*3.567*	*3.520*	
Ru^2-Ru^3	3.573	3.590	3.584	3.545	3.544	3.541
	3.624	*3.524*	*3.561*	*3.527*	*3.514*	
Ru^2-Ru^4	3.627	3.597	3.544	3.550	3.566	3.470
	3.555	*3.579*	*3.484*	*3.486*	*3.504*	
Ru^3-Ru^4	3.639	3.591	3.577	3.536	3.570	3.651
	3.659	*3.653*	*3.628*	*3.617*	*3.636*	
Ru^1-O^1	1.854	1.849	1.842	1.841	1.854	1.899
	1.837	*1.869*	*1.831*	*1.830*	*1.858*	
Ru^1-O^2	1.945	1.933	1.964	1.952	1.926	1.811
	1.929	*1.889*	*1.934*	*1.898*	*1.873*	
Ru^2-O^3	1.855	1.854	1.843	1.854	1.853	1.899
	1.927	*1.903*	*1.837*	*1.848*	*1.855*	
Ru^2-O^4	1.945	1.952	1.932	1.938	1.926	1.811
	1.861	*1.859*	*1.896*	*1.906*	*1.874*	
Ru^3-O^2	1.945	1.954	1.932	1.932	1.926	1.857
	1.861	*1.846*	*1.896*	*1.891*	*1.874*	
Ru^3-O^3	1.855	1.854	1.843	1.842	1.853	1.901
	1.927	*1.920*	*1.837*	*1.836*	*1.855*	
Ru^4-O^1	1.854	1.849	1.842	1.846	1.854	1.902
	1.837	*1.835*	*1.831*	*1.836*	*1.858*	
Ru^4-O^4	1.945	1.933	1.964	1.975	1.926	1.857
	1.929	*1.923*	*1.934*	*1.933*	*1.873*	
Ru^1-O^5	2.012	2.017	1.952	1.978	2.083	2.066
	1.930	*1.970*	*1.945*	*1.977*	*2.063*	
Ru^1-O^6	1.868	1.933	2.013	2.062	2.082	2.061
	1.962	*1.943*	*2.015*	*2.063*	*2.068*	
Ru^2-O^7	1.868	1.903	2.017	2.041	2.082	2.061
	1.949	*1.908*	*2.022*	*2.027*	*2.064*	
Ru^2-O^8	2.012	2.011	1.983	2.050	2.082	2.065
	1.910	*2.035*	*1.981*	*2.025*	*2.053*	
Ru^3-O^9	1.868	1.900	2.017	2.081	2.082	2.072
	1.949	*1.917*	*2.022*	*2.074*	*2.064*	
Ru^3-O^{10}	2.012	2.010	1.983	2.048	2.082	2.042
	1.910	*2.012*	*1.981*	*2.016*	*2.053*	
Ru^4-O^{11}	1.868	1.934	2.013	2.022	2.082	2.073
	1.962	*1.963*	*2.015*	*2.018*	*2.068*	
Ru^4-O^{12}	2.012	2.016	1.952	1.982	2.083	2.042
	1.930	*1.956*	*1.945*	*1.983*	*2.063*	
Ru^1-O^{13}	1.999	1.981	2.004	1.994	1.974	2.004
	2.033	*2.007*	*2.021*	*2.014*	*1.994*	
Ru^2-O^{13}	2.002	1.996	1.978	1.965	1.971	2.003
	1.991	*2.007*	*1.994*	*1.989*	*1.993*	
Ru^3-O^{14}	2.002	1.995	1.978	1.966	1.971	1.993
	1.991	*2.015*	*1.994*	*1.993*	*1.993*	
Ru^4-O^{14}	1.999	1.981	2.004	1.986	1.974	1.993
	2.033	*2.014*	*2.021*	*2.003*	*1.994*	
Ru^1-O^{15}	2.205	2.228	2.227	2.238	2.257	2.072
	2.140	*2.155*	*2.169*	*2.178*	*2.192*	
Ru^2-O^{16}	2.203	2.221	2.242	2.275	2.260	2.072
	2.181	*2.190*	*2.180*	*2.195*	*2.194*	
Ru^3-O^{17}	2.203	2.222	2.242	2.256	2.260	2.130
	2.181	*2.186*	*2.180*	*2.182*	*2.194*	
Ru^4-O^{18}	2.205	2.230	2.227	2.250	2.257	2.129
	2.140	*2.162*	*2.169*	*2.194*	*2.192*	

[a] See Figure 1 for labeling of atoms.

stabilize the HOMOs and LUMOs (see below), provides the same MO picture. The calculated HOMO − (HOMO − 4), LUMO − (LUMO + 4) and HOMO − LUMO energy gaps are 0.294 eV, 1.064, and 0.248 eV at the COSMO level, respectively; these values are smaller than those obtained in the gas-phase. Thus, the calculations show that the $\{Ru_4\}$ core and W−O bonding and antibonding orbitals of the $[\{Ru_4O_4(OH)_2(H_2O)_4\}(\gamma\text{-}SiW_{10}O_{36})_2]^{10-}$ species render a "quasi-continuum" or "nanoparticle-type" character to the frontier orbitals. The observed quasi-continuum nature of the frontier orbitals of **1** closely correlates with experimentally determined oxidation−reduction features and explains the unusual Coulomb staircase structure of its cyclic voltammetry data: seven successive oxidation and reduction potentials that display a linear relationship with the number of electron transferred from or to **1**.[35] Note that a Coulomb staircase is a classical feature of charging a capacitor (an electrode surface, for example) and can be accounted for by simple electrostatic arguments. This phenomenon is rarely observed in molecular systems where electronic coupling usually results in unevenly spaced redox potentials.

TABLE 3: NPA Atomic Charges (in e) of Selected Atoms of the $Ru_4(\mu\text{-}O)_4(\mu\text{-}OH)_2(H_2O)_4$ Core for Compounds 1-5 Calculated at the Gas-Phase and in Water Solution (in italic)[a]

atom	5	4	3	2	1
Ru^1	1.27	1.25	1.23	1.22	1.18
	1.25	*1.25*	*1.24*	*1.22*	*1.18*
Ru^2	1.27	1.26	1.24	1.23	1.19
	1.33	*1.30*	*1.25*	*1.23*	*1.18*
Ru^3	1.27	1.27	1.24	1.20	1.19
	1.33	*1.29*	*1.25*	*1.19*	*1.18*
Ru^4	1.27	1.26	1.23	1.24	1.18
	1.25	*1.26*	*1.24*	*1.23*	*1.18*
O^1	−0.39	−0.38	−0.36	−0.37	−0.40
	−0.34	*−0.38*	*−0.34*	*−0.37*	*−0.44*
O^2	−0.66	−0.65	−0.65	−0.68	−0.65
	−0.48	*−0.45*	*−0.55*	*−0.55*	*−0.52*
O^3	−0.39	−0.39	−0.37	−0.39	−0.39
	−0.52	*−0.50*	*−0.37*	*−0.40*	*−0.44*
O^4	−0.76	−0.65	−0.65	−0.69	−0.65
	−0.48	*−0.50*	*−0.55*	*−0.59*	*−0.52*
O^5	−0.75	−0.76	−0.75	−0.77	−0.81
	−0.67	*−0.69*	*−0.68*	*−0.70*	*−0.73*
O^6	−0.57	−0.64	−0.66	−0.67	−0.68
	−0.68	*−0.70*	*−0.70*	*−0.70*	*−0.70*
O^7	−0.56	−0.61	−0.67	−0.68	−0.68
	−0.65	*−0.63*	*−0.70*	*−0.70*	*−0.70*
O^8	−0.75	−0.75	−0.77	−0.80	−0.81
	−0.63	*−0.70*	*−0.70*	*−0.71*	*−0.73*
O^9	−0.56	−0.61	−0.67	−0.68	−0.68
	−0.65	*−0.64*	*−0.70*	*−0.70*	*−0.70*
O^{10}	−0.75	−0.75	−0.77	−0.80	−0.81
	−0.63	*−0.70*	*−0.70*	*−0.72*	*−0.73*
O^{11}	−0.57	−0.64	−0.66	−0.66	−0.68
	−0.68	*−0.69*	*−0.70*	*−0.69*	*−0.70*
O^{12}	−0.75	−0.76	−0.75	−0.77	−0.81
	−0.67	*−0.68*	*−0.68*	*−0.71*	*−0.73*
O^{13}	−0.72	−0.69	−0.69	−0.68	−0.68
	−0.71	*−0.71*	*−0.71*	*−0.71*	*−0.70*
O^{14}	−0.72	−0.69	−0.69	−0.66	−0.68
	−0.71	*−0.72*	*−0.71*	*−0.70*	*−0.70*
O^{15}	−0.79	−0.81	−0.81	−0.82	−0.84
	−0.78	*−0.80*	*−0.80*	*−0.81*	*−0.82*
O^{16}	−0.79	−0.80	−0.82	−0.83	−0.84
	−0.80	*−0.80*	*−0.81*	*−0.82*	*−0.82*
O^{17}	−0.79	−0.80	−0.82	−0.83	−0.84
	−0.80	*−0.80*	*−0.81*	*−0.82*	*−0.82*
O^{18}	−0.79	−0.81	−0.81	−0.82	−0.84
	−0.78	*−0.80*	*−0.80*	*−0.81*	*−0.82*

[a] For labeling of atoms see Figure 1.

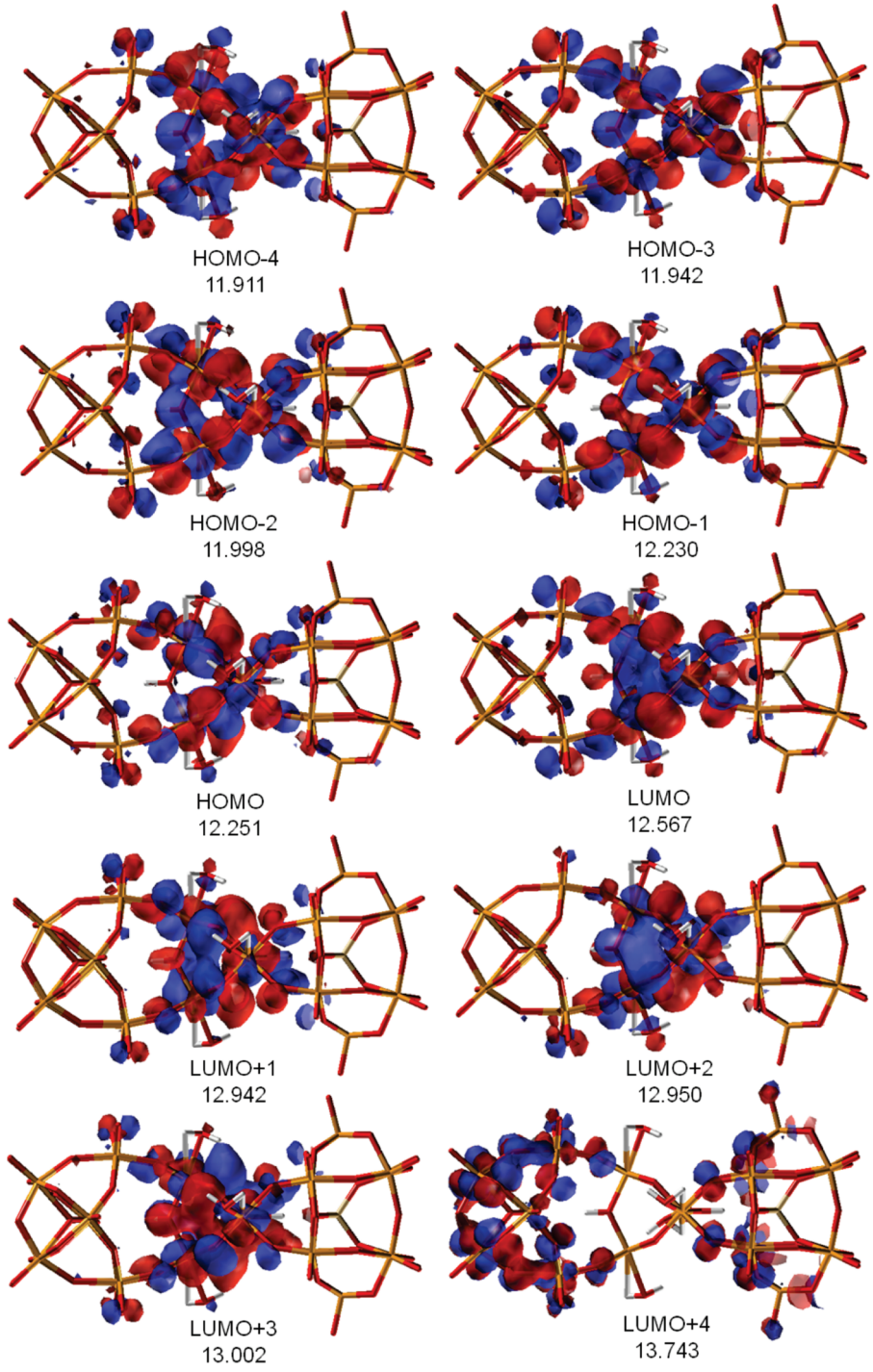

Figure 2. Important HOMOs and LUMOs of **1** and their energies (in eV) computed at the RI-BP86/TZ level of theory.

Some molecular systems, including buckminsterfullerene and a range of platinum carbonyl clusters (26−38 atoms)[36] as well as some gold nanoclusters around 1 nm in diameter[37] also experimentally exhibit several successive redox processes that define a Coulomb staircase. It is interesting to note that in the latter case, the system reverses to a molecule-like behavior (from "bulk-like" behavior) for clusters under 20 kDa (around 100 gold atoms).

In summary, the calculations clearly demonstrate that the sequential removal of four electrons from **1** during redox cycling (catalytic water oxidation/oxygen evolution turnover conditions) involves only the $\{Ru_4\}$ core orbitals. Catalyst instability due to ligand oxidation in the extensively investigated Ru-blue dimer,[8−10,40] $[(bpy)_2(O)Ru^V-(\mu\text{-}O)\text{-}Ru^V(O)(bpy)_2]^{4+}$, and several related complexes,[1,41] is not operable for its "all-inorganic counterpart", **1**. Furthermore, a minimum of four electrons can be reversibly removed from the $\{Ru_4\}$ core orbitals over a narrow range of potentials, which is a situation reminiscent to water oxidation/oxygen evolution catalyzed by the Mn_4CaO_4 cluster in Photosystem II.[1]

Estimation of the Countercation Effect on the Frontier Orbitals of Complex 1. The X-ray crystal structure establishes that in solid state polyanion **1** is neutralized by 10 counter-cations (8 Rb^+ and 2 K^+).[23] In aqueous solution, **1** is almost surely present as a freely diffusing polyanion, but we cannot rule out the presence of some ion pairing particularly at cation high concentration. Unfortunately, explicit ab initio calculations that adequately address the counter-cations are not feasible

TABLE 4: Energies of Frontier Orbitals (in eV) of Compounds 1−5 Calculated at the COSMO Level in Water Solution

		5	4	3	2	1
HOMO − 5	α	−6.411	−6.068	−5.786	−5.477	11.747[a]
	β	−6.659	−6.386	−5.922	−5.446	−5.023
HOMO − 4	α	−6.308	−5.958	−5.696	−5.353	11.911
	β	−6.641	−6.194	−5.661	−5.407	−4.784
HOMO − 3	α	−6.208	−5.920	−5.670	−5.291	11.942
	β	−6.381	−5.969	−5.634	−5.224	−4.882
HOMO − 2	α	−6.147	−5.852	−5.647	−5.210	11.998
	β	−6.170	−5.935	−5.550	−5.186	−4.775
HOMO − 1	α	−6.103	−5.796	−5.429	−5.007	12.230
	β	−6.154	−5.753	−5.491	−5.115	−4.673
HOMO	α	−6.050	−5.685	−5.269	−4.879	12.251
	β	−6.078	−5.714	−5.458	−4.871	−4.490
LUMO	α	−5.471	−5.156	−4.885	−4.533	12.567
	β	−5.644	−5.256	−5.012	−4.610	−4.242
LUMO + 1	α	−5.406	−4.983	−4.719	−4.273	12.942
	β	−5.593	−5.196	−4.892	−4.439	−3.785
LUMO + 2	α	−5.224	−4.952	−4.639	−4.240	12.950
	β	−5.500	−5.144	−4.695	−4.236	−3.766
LUMO + 3	α	−5.219	−4.845	−4.639	−4.086	13.002
	β	−5.441	−4.905	−4.565	−4.121	−3.760
LUMO + 4	α	−4.254	−3.991	−3.707	−3.462	13.743
	β	−5.167	−4.728	−4.463	−4.018	−3.178
LUMO + 5	α	−4.248	−3.976	−3.703	−3.457	13.750
	β	−5.146	−4.668	−4.392	−3.462	−3.175

[a] Numbers given in the first rows of this column are from the gas-phase studies.

computationally. Therefore, we approximate the countercation effect by adding stationary point charges (Q) into the electronic Hamiltonian and solving the resulting Kohn−Sham equations. For this purpose, we have optimized geometry of **1** in D_2 symmetry using the hybrid density functional B3LYP method[34] in conjuction with the standard 6-31G basis set for Si, O, and H and the lanl2dz basis set for Ru and W.[38] The locations of point charges were chosen so as to preserve the D_2 symmetry of **1**−10*Q*, while the charge magnitudes were uniformly scaled to render the entire system electrostatically neutral. We place 10 positive charges ($Q = 0.5$e each) symmetrically over each of the two POM units reflecting the positions of the W atoms and making the corresponding *Q*−W distances uniformly equal to 6 Å. Thus, a total of 20 charges were placed. The shortest distance from a point charge to a terminal oxygen is 3.5 Å. (Cartesian coordinates for the entire system are given in Table S2 of Supporting Information). These calculations were carried out using the Gaussian 03 program.[39]

Comparison of the gas-phase (B3LYP) calculated frontier orbitals of **1** with those obtained in the "point-charge-cage" show that the interactions between **1** and counter-cations stabilize the energies of HOMO and LUMO by ca 0.5 hartree. The stabilization is quite uniform for both the occupied and virtual orbitals. More importantly, the HOMO − LUMO separation is not greatly affected by the applied electric field: it is 0.0091 hartree in the free ion and 0.0069 hartree in the cage. Thus, the conclusions made about the frontier orbitals of **1** based on the gas-phase (or solution phase) studies are also valid for the solid state with 10 counter-cations.

Compound 2, $[\{Ru_4O_4(OH)_2(H_2O)_4\}(\gamma\text{-}SiW_{10}O_{36})_2]^{9-}$. Compound **2** is the product of one-electron oxidation of **1**, where the $\{Ru_4\}$ core has one Ru^V and three Ru^{IV} centers. The ground electronic state of this complex is a doublet with one unpaired electron. Henceforth, in order to avoid redundancy of our discussion, below we will consider only the results obtained with the COSMO approach for compound **2** and all other reported compounds. In Table 2 we present the calculated bond distances for selected atoms of the species **2**. As seen from the table, upon going from **1** to **2**, the geometry of the complex changes only very slightly. The largest differences in bond lengths are 0.086, 0.080, and 0.060 Å for Ru^1-O^5, Ru^4-O^{12}, and Ru^4-O^4 bond distances, respectively. On average, the distance between the $\{Ru_4\}$ core and a $\{SiW_{10}\}$ polyoxoanion is slightly contracted upon going from **1** to **2**. Moreover, the charge distribution within the $\{Ru_4\}$ core remains almost unaltered (Table 3); the charge on Ru centers increases by 0.05e to +1.23e. For the O atoms, the only noticeable changes occur for the O^1 and O^4 centers, the negative charge of which increases by 0.07e. Table 5 provides the NPA spin densities and $\langle S^2\rangle$ values for compound **2**.

TABLE 5: NPA Spin Densities (in e, Only Those Greater or Equal to 0.10e Are Presented) and $\langle S^2\rangle$ Expectation Values for Compounds 2−5 Calculated at the COSMO level (see Figure 1 for Used Labeling Scheme) of Theory in Water Solution

atom	5	4	3	2
Ru^1	−0.12	−0.73	0.19	−0.41
Ru^2	1.32	0.84	0.44	0.76
Ru^3	1.32	0.94	0.44	−0.14
Ru^4	−0.12	0.63	0.19	0.49
O^1		0.11		
O^2	0.10		0.18	−0.10
O^3	0.29	0.19		
O^4	0.10	0.10	0.18	0.17
O^6		−0.10		
O^7	0.17	0.22		
O^8	0.24			
O^9	0.17	0.19		
O^{10}	0.24			
O^{12}		0.11		
$\langle S^2\rangle$	6.21	4.31	2.02	1.13

As seen from Table 5, the spin density is mainly located on the atoms of the $\{Ru_4\}$ core: on all four Ru and two oxygen (O^2 and O^4) centers. This indicates that one electron is removed from the Ru−O bonding orbitals, a finding that is consistent with the frontier orbital picture presented above for compound **1**. Furthermore, analysis of the spin distribution and $\langle S^2\rangle$ values indicates that the calculated doublet ground electronic state of **2** has antiferromagnetically coupled character with some involvement of the higher-lying quartet state, which is calculated to be only 6.1 kcal/mol higher in energy.

The most important features of all α- and β-HOMOs of **2** are qualitatively the same as those reported for **1** addressed above. Thus, removal of one electron from the HOMO of **1** to give **2** keeps all frontier orbitals intact. Inspection of the frontier orbital energies shows that the HOMOs of **2** are also close to each other in energy. The calculated energy gap between the α- and β-components of HOMO and HOMO − 4 is 0.54 eV. The LUMOs of **2** are also clustered, with the energy gap between bottom α- and fifth β-LUMOs within 0.592 eV, respectively. The [α-HOMO] − [β-LUMO] energy gap is 0.269 eV. Comparison of these numbers with the corresponding values for **1** shows that one-electron oxidation of the latter, in general, decreases the continuum-type MO character of this species.

Compound 3, $[\{Ru_4O_4(OH)_2(H_2O)_4\}(\gamma\text{-}SiW_{10}O_{36})_2]^{8-}$. Removal of two electrons from **1** (or one electron from **2**) leads to compound **3**, where the $\{Ru_4\}$ core has two Ru^{IV} and two Ru^V centers. The ground electronic state of **3** is found to be a triplet state. The calculated spin densities (Table 5) show that two unpaired electrons are mainly located on the atoms of the

{Ru_4} core. The calculated $\langle S^2 \rangle$ value, 2.02, is close to its ideal value of 2.0.

As deduced from the geometrical features reported in Table 2, the structures of **2** and **3** are quite similar. The most significant changes in bond distances, 0.048 and 0.052 Å, are found to take place for Ru^1-O^6 and Ru^3-O^9 bonds, respectively. Again, the removal of two electrons from **1** (going to **3**) results in further shortening of the {Ru_4}−{SiW_{10}} distance. The calculated NPA atomic charges are very similar for **3** and **2** (and **1** as well) (see Table 3). The largest change in NPA charges, which is only 0.04e, is found to take place at the O^4 center.

As noted above, compound **3** is formed by the removal of one electron from the SOMO of the compound **2**, which becomes the LUMO in **3**. Therefore, the orbitals having contributions from the {W−O} framework are now α-LUMO + 4 and β-LUMO + 6. In addition, all α-HOMOs and LUMOs remain unaltered relative to those in both **1** and **2**. The calculated energy gaps have the following values: between the β- and α-components of HOMO and HOMO − 4, 0.238 eV; between the β-components of LUMO and LUMO + 4, 0.549 eV; and between the β-components of HOMO and LUMO, 0.446 eV.

Compound 4, $[\{Ru_4O_4(OH)_2(H_2O)_4\}(\gamma\text{-}SiW_{10}O_{36})_2]^{7-}$. Removal of one electron from **3** leads to compound **4** with formally one Ru^{IV} and three Ru^{V} centers, and a quartet ground electronic state with three unpaired electrons. Its sextet electronic state is located only 4.1 kcal/mol higher in energy. As seen in Table 5, unpaired electrons of **4** are mainly located on Ru centers, but also unpaired electron densities larger than 0.10e are present on the O^1, O^3, O^4, O^7, O^9, and O^{12} centers. The calculated $\langle S^2 \rangle$ value of 4.31 is larger than expected value of 3.75, which indicates some mixing of electronic states with higher multiplicities.

In contrast to the cases of compounds **2** and **3**, which result from of one- and two-electron oxidations of **1**, respectively, the removal of the third electron from **1** leads to significant geometrical changes in the product, **4**. Indeed, as seen in Table 2, a substantial elongation of Ru^1-Ru^3 and Ru^2-Ru^4 bond distances by ca. 0.08 Å, and shortening of Ru^1-O^5, Ru^1-O^6, Ru^2-O^7, Ru^3-O^9, Ru^4-O^{11}, and Ru^4-O^{12} bond distances by 0.093, 0.125, 0.156, 0.147, 0.105, and 0.107 Å, respectively, takes place. Consequently, the distance between the {Ru_4} core and {SiW_{10}} fragments is further shortened, on average, upon going to compound **4**. For the Ru_4O_4 core, the largest bond distance variations are 0.048 and 0.065 Å for Ru^2-O^3 and Ru^3-O^3, respectively. The changes in the calculated NPA charges are also noticeable upon going from **1** to **4** (see Table 3): the charges on μ-O_{Ru} centers are decreased by 0.04−0.07e, the charges on Ru centers are increased by 0.07−012e, and the charges on the O centers connecting the {Ru_4} core and {SiW_{10}} fragments are decreased by 0.02−0.10e.

Analysis of the calculated HOMOs and LUMOs for the α- and β-electrons of **4** show that compound **4** is formed by the removal of one β-electron from the HOMO of **3**, leaving the α- frontier orbitals almost intact. As in the compounds **1**−**3**, the HOMOs and LUMOs of **4** are quite close in energy. The following values of the energy gaps were found: between the β-components of HOMO and HOMO − 4, 0.48 eV; β-components of LUMO and LUMO + 4, 0.528 eV; and β-components of HOMO and LUMO, 0.458 eV.

Compound 5, $[\{Ru_4O_4(OH)_2(H_2O)_4\}(\gamma\text{-}SiW_{10}O_{36})_2]^{6-}$. Oxidation of all Ru^{IV} centers in **1** to Ru^{V} leads to the formation of compound **5**. The calculations show that compound **5** has a quintet ground electronic state. Its nonatet state is located 8.1 kcal/mol higher in energy. As seen in Table 5, all unpaired electrons are localized on Ru as well as on μ-O_{Ru} and μ-O_W centers. The calculated $\langle S^2 \rangle$ value of 6.21 is close to the expected value of 6.0. Furthermore, upon going from **4** to **5** the positive charges on Ru centers are slightly increased and negative charges on μ-O_W centers are slightly decreased. These changes in NPA charge distribution are consistent with the geometry changes upon going from **4** to **5**: in average, the distance between the {Ru_4} core and {SiW_{10}} fragments contract further.

The calculated frontier orbitals of **5** are, again, close in energy. The energy gap between the β-components of HOMO and HOMO − 4 is 0.563 eV; between the β-components of LUMO and LUMO + 4 is 0.477 eV, and between the β-components of HOMO and LUMO is 0.434 eV.

Conclusions

From the above discussion one may draw the following conclusions:

(1) The RI-BP86 method with the DZ or TZ quality basis sets appropriately describes the geometry and low-lying electronic states of compound **1**. The hybrid B3LYP approach overestimates the high-spin states over the low-spin states. Inclusion of the solvent and/or countercation effects into calculations improves the agreement between the calculated and experimental values of geometry parameters, stabilizes the frontier orbitals, but does not change the important conclusions drawn from the gas-phase study results.

(2) The most closely lying HOMOs and LUMOs of complex **1** are characterized to be bonding and antibonding MOs of the $[Ru_4(\mu\text{-}O)_4(\mu-OH)_2(H_2O)_4]^{6+}$ core. Therefore, four subsequent one-electron oxidations of **1** leading to complexes **2, 3, 4**, and **5**, respectively, effectively involve only the {Ru_4} core orbitals. In other words, catalyst instability due to ligand oxidation in the heavily studied Ru-blue dimer,[7,8,10,40] $[(bpy)_2(O)Ru^{V}\text{-}(\mu\text{-}O)\text{-}Ru^{V}(O)(bpy)_2]^{4+}$, is not operable for the tetra-ruthenium polytungstate water oxidation catalyst, **1**, which represents in some central aspects, an all-inorganic counterpart of the blue dimer. It is predicted that complex **1** will be stable during the $4e^-$ water oxidation process catalyzed by **1**.

(3) The {Ru_4} core and {W−O} bonding and antibonding HOMOs and LUMOs of **1** are very close in energy and exhibit quasi-continuum or nanoparticle-type character. This conclusion closely correlates with the experimentally reported oxidation and reduction properties of **1** and explains the unusual Coulomb staircase structure of the sequential features in the cyclic voltammograms of this species.[23,35] The decrease in total negative charge of the system via **1** > **2** > **3** > **4** > **5** does not alter this conclusion.

(4) The decrease in total negative charge of the system via **1** > **2** > **3** > **4** > **5**, on average, decreases the {Ru_4}−{SiW_{10}} distance, whereas it does not significantly change geometry parameters within the {Ru_4} core or the {SiW_{10}} polyoxoanion. The basicity of the {Ru_4} core oxygen atoms (i.e., {$Ru_4O_4(OH)_2(H_2O)_4$}), as well as of {Ru_4}−{SiW_{10}} linkage oxygens increases via μ-O_{Ru} < $\mu-OH_{Ru}$ < μ-O_W < O_{water}. It is predicted that at higher pH values, compound **1** will initially release protons from the μ-OH_{Ru} oxygen centers.

Acknowledgment. The present research is supported by the U.S. Department of Energy (grant DE-FG02-03ER15461). The use of computational resources at the Cherry Emerson Center for Scientific Computation is also acknowledged.

Supporting Information Available: (Total of 14 pages) includes: (a) Completed ref. 39, (b) Cartesian coordinates (in Å) of all studied complexes at their ground electronic states

calculated at the RI-BP86 and COSMO levels of theory (Table S1), and (c) Cartesian coordinates (in Å) of **1** in "point-charge-cage" (point charges are labeled as "He") (Table S2). This material is available free of charge via the Internet at http://pubs.acs.org.

References and Notes

(1) Eisenberg, R.; Gray, H. B. *Inorg. Chem.* **2008**, *47*, 1697–1699, references therein, and this entire issue.

(2) Ramaraj, R.; Kira, A.; Kaneko, M. *Chem. Lett.* **1987**, *16*, 261–264.

(3) Elizarova, G. L.; Zhidomirov, G. M.; Parmon, V. N. *Catal. Today* **2000**, *58*, 71–78.

(4) Hammarström, L.; Sun, L.; Åkermark, B.; Styring, S. *Catal. Today* **2000**, *58*, 57–69.

(5) Hoertz, P. G.; Kim, Y.; Youngblood, W. J.; Mallouk, T. E. *J. Phys. Chem. B* **2007**, *111*, 6845–6856.

(6) Gersten, S. W.; Samuels, G. J.; Meyer, T. J. *J. Am. Chem. Soc.* **1982**, *104*, 4029–4030.

(7) Gilbert, J. A.; Eggleston, D. S.; Wyatt, R. M., Jr.; Geselowitz, D. A.; Gersten, S. W.; Hodgson, D. J.; Meyer, T. J. *J. Am. Chem. Soc.* **1985**, *107*, 3855–3864.

(8) Schoonover, J. R.; Ni, J. F.; Roecker, L.; White, P. S.; Meyer, T. J. *Inorg. Chem.* **1996**, *35*, 5885–5892.

(9) Sens, C.; Romero, I.; Rodríguez, M.; Llobet, A.; Parella, T.; Benet-Buchholz, J. *J. Am. Chem. Soc.* **2004**, *126*, 7798–7799.

(10) Hurst, J. K. *Coord. Chem. Rev.* **2005**, *249*, 313–328.

(11) Zong, R.; Thummel, R. *J. Am. Chem. Soc.* **2005**, *127*, 12802–12803.

(12) Rüttinger, W.; Dismukes, G. C. *Chem. Rev.* **1996**, *97*, 1–24.

(13) Limburg, J.; Vrettos, J. S.; Liable-Sands, L. M.; Rheingold, A. L.; Crabtree, R. H.; Brudvig, G. W. *Science* **1999**, *283*, 1524–1527.

(14) Yagi, M.; Kaneko, M. *Chem. Rev.* **2001**, *101*, 21–35.

(15) Chen, H.; Faller, J. W.; Crabtree, R. H.; Brudvig, G. W. *J. Am. Chem. Soc.* **2004**, *126*, 7345–7349.

(16) Tagore, R.; Chen, H.; Zhang, H.; Crabtree, R. H.; Brudvig, G. W. *Inorg. Chim. Acta* **2007**, *360*, 2983–2989.

(17) Tagore, R.; Crabtree, R. H.; Brudvig, G. W. *Inorg. Chem.* **2007**, *46*, 2193–2203.

(18) Pecoraro, V. L.; Hsieh, W.-Y. *Inorg. Chem.* **2008**, *47*, 1765–1778.

(19) Siegbahn, P. E. M. *Inorg. Chem.* **2008**, *47*, 1779–1786.

(20) Dubé, C. E.; Wright, D. W.; Pal, S.; Bonitatebus, P. J.; Armstrong, W. H. *J. Am. Chem. Soc.* **1998**, *120*, 3704–3716.

(21) Mukhopadhyay, S.; Mandal, S. K.; Bhaduri, S.; Armstrong, W. H. *Chem. Rev.* **2004**, *104*, 3981–4026.

(22) Ferreira, K. N.; Iverson, T. M.; Maghlaoui, K.; Barber, J.; Iwata, S. *Science* **2004**, *303*, 1831–1838.

(23) Geletii, Y. V.; Botar, B.; Kögerler, P.; Hillesheim, D. A.; Musaev, D. G.; Hill, C. L. *Angew. Chem., Int. Ed.* **2008**, *47*, 3896–3899.

(24) Sartorel, A.; Carraro, M.; Scorrano, G.; Zorzi, R. D.; Geremia, S.; McDaniel, N. D.; Bernhard, S.; Bonchio, M. *J. Am. Chem. Soc.* **2008**, *130*, 5006–5007.

(25) Becke, A. D. *Phys. Rev. A* **1988**, *38*, 3098–3107.

(26) Perdew, J. P. *Phys. Rev. B* **1986**, *33*, 8822–8824.

(27) (a) Schäfer, A.; Huber, C.; Ahlrichs, R. *J. Chem. Phys.* **1994**, *100*, 5829–5835. (b) Eichkorn, K.; Weigend, F.; Treutler, O.; Ahlrichs, R. *Theor. Chem. Acc.* **1997**, *97*, 119–124.

(28) Eichkorn, K.; Treutler, O.; öhm, H.; Häser, M.; Ahlrichs, R. *Chem. Phys. Lett.* **1995**, *242*, 652–660.

(29) Arnim, M. v.; Ahlrichs, R. *J. Comput. Chem.* **1998**, *19*, 1746–1757.

(30) Klamt, A.; Schüürmann, G. *J. Chem. Soc. Perkin Trans.2* **1993**, *5*, 799–805.

(31) Ahlrichs, R.; Bär, M.; Hacer, M.; Horn, H.; Kömel, C. *Chem. Phys. Lett.* **1989**, *162*, 165–169.

(32) Schaftenaar, G.; Noordik, J. H. *J. Comput. Aid. Mol. Design* **2000**, *14*, 123–134.

(33) Schäfer, A.; Horn, H.; Ahlrichs, R. *J. Chem. Phys.* **1992**, *97*, 2571–2577.

(34) (a) See ref. 25; (b) Lee, C.; Yang, W.; Parr, R. G. *Phys. Rev. B* **1988**, *37*, 785–789.

(35) Geletii, Y. V.; Besson, C.; Hou, Y.; Yin, Q.; Musaev, D. G.; Quinonero, D.; Cao, R.; Hardcastle, K. I.; Proust, A.; Kögerler, P.; Hill, C. L. *J. Am. Chem. Soc.* **2009**, *131*, 17360–17370.

(36) (a) Roth, J. D.; Lewis, G. J.; Safford, L. K.; Jiang, X.; Dahl, L. F.; Weaver, M. J. *J. Am. Chem. Soc.* **1992**, *114*, 6159–6169. (b) Weaver, M. J.; Gao, X. *J. Phys. Chem.* **1993**, *97*, 332–338.

(37) (a) Ingram, R. S.; Hostetler, M. J.; Murray, R. W.; Schaaff, T. G.; Khoury, J. Y.; Whetten, R. L.; Bigioni, T. P.; Guthrie, D. K.; First, P. N. *J. Am. Chem. Soc.* **1997**, *119*, 9279–9280. (b) Chen, S.; Murray, R. W.; Feldberg, S. W. *J. Phys. Chem. B* **1998**, *102*, 9898–9907. (c) Chen, S.; Ingram, R. S.; Hostetler, M. J.; Pietron, J. J.; Murray, R. W.; Schaaff, T. G.; Khoury, J. T.; Alvarez, M. M.; Whetten, R. L. *Science* **1998**, *120*, 2098–2101.

(38) (a) Hay, P. J.; Wadt, W. R. *J. Chem. Phys.* **1985**, *82*, 270–283. (b) Hay, P. J.; Wadt, W. R. *J. Chem. Phys.* **1985**, *82*, 299–310. (c) Wadt, W. R.; Hay, P. J. *J. Chem. Phys.* **1985**, *82*, 284–298.

(39) Frisch, M. J.; Trucks, G. W.; Schlegel, H. B.; Scuseria, G. E.; Robb, M. A.; Cheeseman, J. R.; Montgomery, J. A., Jr.; Vreven, T.; Kudin, K. N.; Burant, J. C.; Millam, J. M.; Iyengar, S. S.; Tomasi, J.; Barone, V.; Mennucci, B.; Cossi, M.; Scalmani, G.; Rega, N.; Petersson, G. A.; Nakatsuji, H.; Hada, M.; Ehara, M.; Toyota, K.; Fukuda, R.; Hasegawa, J.; Ishida, M.; Nakajima, T.; Honda, Y.; Kitao, O.; Nakai, H.; Klene, M.; Li, X.; Knox, J. E.; Hratchian, H. P.; Cross, J. B.; Bakken, V.; Adamo, C.; Jaramillo, J.; Gomperts, R.; Stratmann, R. E.; Yazyev, O.; Austin, A. J.; Cammi, R.; Pomelli, C.; Ochterski, J. W.; Ayala, P. Y.; Morokuma, K.; Voth, G. A.; Salvador, P.; Dannenberg, J. J.; Zakrzewski, V. G.; Dapprich, S.; Daniels, A. D.; Strain, M. C.; Farkas, O.; Malick, D. K.; Rabuck, A. D.; Raghavachari, K.; Foresman, J. B.; Ortiz, J. V.; Cui, Q.; Baboul, A. G.; Clifford, S.; Cioslowski, J.; Stefanov, B. B.; Liu, G.; Liashenko, A.; Piskorz, P.; Komaromi, I.; Martin, R. L.; Fox, D. J.; Keith, T.; Al-Laham, M. A.; Peng, C. Y.; Nanayakkara, A.; Challacombe, M.; Gill, P. M. W.; Johnson, B.; Chen, W.; Wong, M. W.; Gonzalez, C.; Pople, J. A. *Gaussian 03*, revision D1; Gaussian, Inc.: Wallingford, CT, 2004.

(40) Yang, X.; Baik, M.-H. *J. Am. Chem. Soc.* **2006**, *128*, 7476–7485.

(41) Romain, S.; Bozoglian, F.; Sala, X.; Llobet, A. *J. Am. Chem. Soc.* **2009**, *131*, 2768–2769.

JP907471H